Title
THE ENERGY SPECTRUM OF THE POSITRONS FROM K-+MESON DECAY

Authors
Sagane, Ryokichi
Gardner, William L.
Hubbard, Harmon W.

Publication Date
1951-06-15

UCRL-1261 REV
UNCLASSIFIED

UNIVERSITY OF CALIFORNIA — BERKELEY

RADIATION LABORATORY

DISCLAIMER

UCRL-1261 Rev.
Unclassified-Physics Distribution

UNIVERSITY OF CALIFORNIA

Radiation Laboratory

Contract No. W-7405-eng-48

THE ENERGY SPECTRUM OF THE POSITRONS FROM μ^+ MESON DECAY

Ryokichi Sagane, William L. Gardner
and Harmon W. Hubbard

June 15, 1951

Berkeley, California

UCRL-1261 Rev.
Unclassified-Physics Distribution

THE ENERGY SPECTRUM OF THE POSITRONS FROM μ^+ MESON DECAY

Ryokichi Sagane, William L. Gardner
and Harmon W. Hubbard

Radiation Laboratory, Department of Physics
University of California, Berkeley, California

June 15, 1951

ABSTRACT

The energies of the positrons from μ^+ meson decay are measured in a Spiral Orbit Spectrometer. The mesons are produced by the 340 Mev protons from the Berkeley 184-inch Cyclotron. The spectrometer employs a particle orbit of 21 inches diameter with magnetic fields as high as 20,000 guass. The positrons are detected by scintillation crystals in quadruple coincidence. A considerable increase in the accuracy of the positron momentum spectrum is obtained.

UCRL-1261 Rev.
Unclassified-Physics Distribution

THE ENERGY SPECTRUM OF THE POSITRONS FROM μ^+ MESON DECAY

Ryokichi Sagane, William L. Gardner
and Harmon W. Hubbard

Radiation Laboratory, Department of Physics
University of California, Berkeley, California

June 15, 1951

I. INTRODUCTION

An investigation of the energy of the electrons resulting from the decay of μ mesons has been conducted using a relatively new technique. Mesons produced artifically by protons from the 184-inch cyclotron are used as the source of positrons, and the energies of these positrons are measured in a "Spiral Orbit Spectrometer".

This type of spectrometer has been studied and developed in Japan[1] since 1941. The present experiment is the first application of this technique in this country.

The relatively high counting rate permits a considerable extension in the accuracy of the spectrum as given by previous research.[2,3,4] All the former work has been done with cosmic ray mesons as a source. The combination of the cyclotron beam and the spiral orbit spectrometer has enabled us to conduct a controlled experiment on the energy spectrum.

The external deflected beam of 340 Mev protons from the cyclotron produces π mesons of both plus and minus variety. We are interested primarily in the π^+ meson production. The cross section for π^+ production by protons has been investigated by Richman[5] and others. The target of the cyclotron beam is located at the source position of the spectrometer. π^+ mesons which stop in the target give rise to μ^+ mesons through $\pi^+ \rightarrow \mu^+ + \nu$ decay process

with a mean life of 2.6×10^{-8} seconds.[6] The 4 Mev energy of the μ^+ meson is absorbed in approximately 0.2 grams/cm^2 and therefore almost all of these mesons remain in the target. Their decay with a mean life of 2.15×10^{-6} seconds[7,8] gives rise to the positrons, and the magnetic field of the spectrometer is employed to define a particular energy interval of the energy spectrum present. The positrons are detected by four scintillation crystals and associated photomultiplier tubes in quadruple coincidence.

II. APPARATUS

Spiral Orbit Spectrometer

The "Spiral Orbit" spectrometer has been given this name because of the manner in which the particles, of a particular momentum, emerging from the center, spiral outward and approach to the so called "stable orbit". Particles of a lower momentum will be turned back before reaching the orbit, and will return to the origin. Particles of a higher momentum will go out, pass through the orbit, and be lost. The rapidity with which a particle of the correct momentum reaches the orbit is of course dependent on the particular magnetic field distribution employed. For a field distribution similar to that labeled "B" in Figure 1, it has been demonstrated[9] that a particle of a momentum to be focused in the orbit is already close to the orbit after it has been turned through less than 180° from its original angle of emission. And a particle of momentum only 10 percent lower will have a maximum travel out from the center of less than 6/10 of the radius to the orbit, and is then deflected back to the origin. A critical stability exists for particles in the "stable" orbit. After a few traversals of the circular orbit, they are lost.

In order to have a spiral orbit, and the charged particle approach to a

circle of radius $r = \rho$, the following conditions should be satisfied at $r = \rho$;

$$\frac{dr}{dt} = 0, \text{ and } \frac{d^2r}{dt^2} = 0 \tag{1}$$

Therefore, as indicated by Iwata, Miyamoto, and Katani,[1]

$$mv = eA\rho \ , \tag{2}$$

$$H_r = \rho\rho^2 = \int_0^\rho H(r)\, rdr \tag{3}$$

are the definition of the stable orbit, and of the momentum of a charged particle in that orbit. A salient feature of this equation is the fact that the position of the stable orbit is determined by the shape of the magnetic field distribution, and is completely independent of the absolute magnitude of the field. (This is true as long as the field shape does not change when H_{max}, i.e. the current setting, is changed.)

Examples of the field distributions employed are given in Figure 1. The B field distribution (associated with a 3-1/4 inch pole gap) was used in the early stages of the experiment. It has the advantage of quite large vertical focusing, with a resultant increase in the detection efficiency. The field distribution labeled A (associated with a gap of 2-5/8 inches) has practically no verticle focusing, as can be seen from the graph, except in the vicinity of the orbit. But it has the advantage of an H value at the orbit large enough to cover the upper end of the spectrum ($<$ 50 Mev electrons). The presence of a homogeneous magnetic field in a major part of the gap also permits the employment of the proton moment nuclear fluxmeter for an accurate absolute calibration of the field. The position of the stable orbit is determined from Equation (3) by numerical integration. A field distribution of the type A above also improves the accuracy in the calculation of ρ.

A plan view of the cyclotron, deflected beam, and positioning of the

spectrometer is shown in Figure 2. The proton beam is collimated with a 4 foot long brass collimator of 1/2 inch internal diameter. The targets used were: Be 1-1/8 in. diameter x 3-1/4 in. long; C 1 in. diameter x 3 in. long; Al 1 in. diameter x 3 in. long. One and 1/4 inch holes were located in each of the pole pieces, coincident with the axis of the magnetic field, for the passage of the beam.

Figure 3 is a photograph of the spectrometer. The iron pole pieces and the iron bars and plates of the flux return path were added in order to give an efficient shape to the field distribution in the gap, as well as to increase the absolute magnitude of the field, thus extending the upper energy limit of the spectrometer. Currents as high as 800 amperes were used with peak fields of about 20,000 gauss. The pole pieces are 20 inches in diameter, and the total weight of the spectrometer is about 6 tons.

Scintillation Detection of Particles

For the detection of particles in the orbit, scintillation crystals and photomultiplier tubes were used. Figure 4 shows the arrangement of the detecting apparatus in the spectrometer. Quite clear anthracene crystals of dimensions 1-1/4 in. x 3/4 in. x 3/16 in. were placed on one end of Lucite light pipes. Crystal and pipes were enclosed in reflecting aluminum foil, and the whole was wrapped with black tape. The photomultiplier tubes (1P21) were encased in a close-fitting magnetic shield of 1/2 inch iron, slotted for insertion of the light pipe. These shields were effective in the somewhat large field gradients present at the flux cross-over region. Tests indicated that the phototube efficiency variation as a function of magnetic field setting was less than 3 percent over the entire range. The final crystal and phototube mount is shown in the photograph of Figure 5. Four crystal detectors

were used, with a central angle of 15° between crystals. A particle moving in a straight line, will be unable to traverse the four crystals. C $\longrightarrow$ electronic circuits. The electronic counting arrangement is presented in Figure 6. Signals from the phototube go into a Discriminator and Pulse Former Circuit (of resolving time 0.2 μ sec.). At maximum sensitivity a 40 millivolt or larger pulse will trip these circuits and the output pulse is a uniform 30 volts. These pulses are then fed into a Quadruple Coincidence circuit (of resolving time 0.2 μ sec.). The high voltage on the phototubes was usually in the vicinity of 1250 volts.

In order to identify these quadruple coincidences with the positrons of μ^{+} decay, we require that their decay have the characteristic half-life. For this reason the quadruple coincidence signals are again fed into coincidence with 2 μ sec. gates so that the counting rate decay over 2 μ sec. intervals may be observed. The cyclotron beam has a repetition rate of $\sim$60 pulses per second, and each pulse of the electrically deflected beam has a duration of less than 0.3 μ sec. The deflector pulse triggers the gate forming units. The position of the start of these tandem gates can be varied, and it was usually found desirable to delay the counting until about 5 μ sec. after the beam pulse. With a mean life of 2.15 μ sec., this obviously indicates a large loss in total counts obtainable. But the high singles counting rate during and immediately after the beam resulted in a rather high accidental quadruple background counting rate, which could be effectively eliminated only by the insertion of this delay.

The source of this large singles counting rate is not very well understood. A large neutron flux is known to exist in the shielded cave of the external beam port. Recoil protons and neutron induced activities are undoubtedly a major factor. Any intense short lived γ activity of the target itself might contribute to accidental quadruples. In addition the disproportionately

large signal due to the actual beam flux is occasionally capable of rendering the electronic detecting apparatus inoperative for as long as 3 microseconds.

Background Determination

Several methods of determination of the background counting rate were investigated, and the two most unambiguous methods are sketched in Figure 7. In the test labeled A, a 4 inch thick piece of lead, - large enough to completely cover the crystal, was placed in the orbit immediately above the top crystal. It did not block the crystals from any radiation from the target, nor in general from any other direction except that of the orbit. The test labeled B consisted of removing alternate crystals radially back out of the orbit 1 inch. The crystals were 3/4 inch wide (dimension along the radius) so that this travel made it impossible for a particle in the orbit to give a quadruple coincidence. And yet the exposure of the crystals to all general background radiation was not diminished.

Operational Procedure

The integration of the cyclotron beam was accomplished by the use of an ion chamber coupled into an integrating electrometer.[10] The ion chamber was filled to 100 cm of argon - CO_2 mixture, and was checked for linearity with beam intensity.

Under normal operating conditions the magnet current setting corresponding to a particular momentum interval would be maintained until a convenient charge was indicated on the electrometer. The exposure time would be of the order of 5 minutes. The electrometer was then cleared and a new momentum interval observed for the same total beam charge. In this manner the total momentum spectrum was covered in a relatively short period, and then

the entire process would be repeated, usually about four times. This method served to eliminate long term drift effects as well as to permit a constant check on the reproducibility of the data. The position of the start of the counting and the beam intensity were adjusted until the background counting rate, as determined by the above tests, was less than 5 percent of the normal rate. The cyclotron beam intensity would occasionally be lowered by a factor of 1/2 and 1/4 and the runs repeated to ascertain that the observed counts were real events.

III. EXPERIMENTAL RESULTS

The results of the several experimental runs with the cyclotron are embodied in the graphs of Figures 8 and 9. In Figure 8 the experimental data are plotted as actually observed, - making only the initial correction of $I = \frac{I_{OBSERVED}}{H\rho}$ for a spectrometer. In Figure 9 these data have been corrected for the energy resolution peculiar to this instrument. The shape of the resolution curve is also included on the graph. A discussion of the accuracy of this correction is incorporated in the following section.

A total of about 4,000 counts were obtained for this spectrum determination. Some idea of the counting rate can be given by the data from a recent run wherein the counting rate, for a magnetic field setting corresponding to $p = 70\ m_e c$, (momentum units in electron masses times c) was in the vicinity of 7 counts/min.

The agreement of the decay of the observed counting rate with that for μ^+ meson decay is portrayed in Figure 10. All of the counts for the run considered are totaled for each successive gate and the counting rate given is the individual total for the respective gate. The slope of the line is arbitrarily drawn for $\tau_{mean} = 2.15\ \mu$ sec. as given by Nereson and Rossi.[7]

IV. ACCURACY OF THE MEASUREMENTS

Magnetic Field and Orbit Determinations

The measurements of the absolute intensity of the magnetic field were done with a nuclear fluxmeter which is sufficiently accurate that the error in this determination is negligible. The magnet current was adjusted by the use of a current regulator attached to the generator. Repetition of the measurements for the same setting of the magnet current has shown that the reproducibility is better than 1 percent. The change in field distribution against radius with different magnet currents was checked to be less than the error of the flip coil measurements which is of the order of $\pm$ 1 percent to 2 percent.

Evaluation of Additional Background Effects

Other types of errors are also to be considered:

1. Very energetic beta ray activity produced at the target.
2. Electrons from μ^- decay.
3. Superposition of positrons produced at the first crystal due to π^+ mesons stopping in the first crystal and giving rise to $\pi^+ \rightarrow \mu^+$ decay and $\mu^+ \rightarrow e^+$ decay.
4. Effect of scattering of the electrons at the crystals and also during flight in 1 atmosphere pressure over a path length of 2 feet to 3 feet.
5. Effect of energy loss of the electrons going through matter both at the target, and at the crystals.

Fortunately, all these errors have been checked to be small in the region of the momentum spectrum, i.e. from 40 to 110 $m_e c$. The method of investigation

of each effect was as follows:

1. Since the spectrometer is symmetric to charged particles of either sign, it is possible to have quadruple coincidences from negative particles of the same momentum as that of the positrons under observation. Therefore any beta activity in this momentum range would give rise to real counts. However, theoretical considerations indicate that beta activity with a beta energy $>$ 20 Mev is extremely unlikely. Due to the difficulty of measurement there is not much experimental data on this subject. It is apparent though that our experimental arrangement was simultaneously a feasible method of making such an investigation. The magnitude of such possible contamination was shown to be quite small by these tests;
   a) by counting with reduced energy of the proton beam. The yield of π^+ mesons is supposed to be very sensitive to the proton energy[10] while the beta ray activity is expected to be about the same, i.e. relatively independent of the proton energy in the region of 300 to 340 Mev.
   b) by counting with targets of different elements. The energy spectra for Be, C, and Al targets were the same within the statistical error, and one would expect that the energies and intensities of any contaminating beta activities would be quite sensitive to the target element.
2. Again because of the acceptance of the spectrometer of both + and - charged particles any $\mu^- \rightarrow e^-$ decay would be included in with the $\mu^+ \rightarrow e^+$ decay. Of course because of the large capture probability of the π^- in the target material this effect was expected to be quite small. This fact was corroborated by placing a 4 inch Pb absorber below the bottom crystal, (similar to the background test discussed earlier as applied to

the top crystal) and the relatively small change in the counting rate (less than 5 percent) would be accounted for by the slight decrease in the transmission solid angle of the spectrometer.

3. Effect of π^+ stopping and decaying in the first crystal. It should be noted that the spectrometer focuses π mesons of a corresponding $H\rho$. Indeed, this property was employed in an earlier experiment for a determination of the π^+/π^- ratio in a single emulsion.[11] The π^+ energy corresponding to an $H\rho$ of $p = 100\ m_e c$ is approximately 12 Mev. Approximately 1.2 gm/cm^2 of Cu will stop these mesons, and such an absorber was placed in the orbit about 8 inches from the first crystal. Any real counts due to this source would drop off by approximately the ratio of the solid angle subtended by the crystals for the old and new positions of the meson absorber. The counting rate change was slight, so evidently the original small solid angle kept this effect small.

4. Scattering of electrons. This was tested by putting an additional crystal, 7/8 inch thick in front of the first one. It is calculated that this will exaggerate the scattering by a factor of three. The counting rate indicated however that even this accentuated effect is less than 8 percent, so that the actual effect of scattering in the regular crystals should not be an important factor. The pole gap enclosure was not evacuated so that the average 2 foot or 3 foot trajectory of the particle was through that amount of normal atmosphere. The long path magnifies the effect of the scattering, but the small amount of matter traversed ($\sim$0.03 gm/cm^2) together with the particle energies involved ($\sim$35 Mev) are the basis for the estimate that the air scattering is less than that in the crystals which was tested to be small.

5. Energy loss in crystals and in target. The energy loss due to ionization per crystal is calculated to be close to 0.8 Mev over the momentum range

considered. The main effect of this loss is the tendency for the particle to leave the orbit due to the lowered momentum. However, this momentum change is relatively small, (for a 40 Mev positron, this corresponds to a 2 percent momentum change). Moreover, since this energy loss per crystal is relatively constant for a 30-50 Mev positron, the net effect of this momentum shift will be a slight decrease in the detection efficiency which will not change the shape or position of the spectrum. The mean radiation losses over this momentum range for carbon, (main constituent of the scintillation crystals) is less than 1/5 the ionization losses so this effect can be considered as negligible.

Energy losses in the target, though, are more important. The mean thickness of target material traversed by the positrons is calculated by considering; 1) the efficiency of the spiral orbit spectrometer for sources made up of cylindrical shells of varying radii, and 2) the radial density distribution of μ^+ decay in the target. For the case of a beryllium target, the radiation loss compared to the ionization loss is relatively smaller than for the case of carbon mentioned above. These considerations lead to an estimate of 0.25 inch as the mean target thickness traversed with an overall average energy loss of 2 Mev. This correction is included in both spectrum plots.

6. Miscellaneous sources. As for the electrons due to the γ rays produced, by capture of π^-, or π^0 decay, these are eliminated by starting the counting only after a decay of several microseconds.

The percentage of π^+ mesons which decay directly into positrons is extremely small,[12] and any such positron counts are similarly eliminated by the use of delay gate circuits.

Resolution Curve of Spectrometer

One of the most important points that should be discussed here is the resolution curve of the spectrometer. There will be a spread in the resolution curve due to the effect of the comparatively large diameter of the target and also added to this will be the electron contribution of the pole surfaces. This latter effect may be appreciable, especially in the region close to the axis because the density of π mesons absorbed in this region is expected to be rather high. The π mesons thus absorbed may result in a moderate electron emission from the pole surfaces.

The ratio of the target radius to the radius of the critical orbit should be less than 0.03; and for maximum energy resolution, as low as 0.01. In order to obtain a reasonable counting rate, a rather large target was used, for which the ratio was 0.05. However, the effective ratio is smaller than this due to the collimation which results in a higher beam density at the center of the target. The ratio should be close to 0.04, and for the detector system used, this corresponds to an energy resolution of about ± 5 percent. The resolution of the spectrometer is rather sensitive to the central angle subtended by the system. In this apparatus the angle was 45°, which is sufficiently large that it helps offset the spread due to the large diameter target. The ratio of crystal detector width to the radius of the orbit is 1/15. The energy resolution is relatively insensitive to the crystal width in this region (e.g. a 50 percent increase in detector width would affect the energy resolution less than 10 percent). Since an increase in the crystal width would increase the overall detection efficiency, such a possibility had been considered. But the drop in light collection efficiency for such a crystal would offset most of this gain.

In order to study the spread due to electrons from the pole surfaces, two tests were conducted, as sketched in Figure 11. In the test labeled A, two Be targets were employed, both of 1-1/8 inch diameter. The first one, 1 inch long was positioned such that it was forward of the gap with its rear surface flush with the gap. The second one, 3 inches long, was back of the gap, and with its front surface flush. With this arrangement the number of mesons absorbed by the pole piece surfaces in question is estimated to be of the order of one-half of normal, and of course the counts due to electrons from the target will be completely missing. The test labeled B consisted of taking data with the target in its normal position and with removable cones as shown, first in position, - and then with them completely out of the gap. The electron contribution of the pole pieces should be considerably decreased by the absence of these particular pole surfaces. The information obtained from these tests is that the background counts due to this effect of the pole surfaces is less than 1/10 of the total area of the resolution curve.

The proton beam density at the target is also an important factor in the shape of the resolution curve. The usual beam collimator employed was 4 feet long and 1/2 inch internal diameter. This resulted in a fairly homogeneous beam of 3/4 inch at the target, and considerable time was always given for the precise adjustment of this beam on the target center. This gives a denser population of π mesons close to the axis of the 1-1/8 inch diameter target which tends to diminish the otherwise expected resolution spread. So from the combined results of both calculations and tests mentioned above the resolution curve as given in Figure 9 is considered to be the most likely one.

The corrections due to this resolution curve are very small for the momentum spectrum around the intensity maximum, but are large for points close to the momentum maximum. So it might be pointed out that the error in the esti-

mation of the resolution curve does not affect the momentum value of I_{max} over 1 percent to 2 percent, - but may affect the momentum value of E_{max} about 3 to 4 percent.

Conclusions

The momentum spectrum obtained is shown in Figures 8 and 9. The momentum value for the intensity maximum is $p = 72 \pm 3\ m_e c$.

The nature of the μ meson and its decay products are discussed by Tiomno, Wheeler, and Rau[13], and more recently by Michel.[14] Although the process of μ^+ meson decay yielding a neutral meson $\mu^+ \rightarrow e^+ + \mu o + \nu$, of small rest mass cannot be ruled out, the process $\mu^+ \rightarrow e^+ + 2\nu$ is the favored reaction.[15] In an examination of the experimental spectrum as compared to the theoretical curves[13] for simple types of coupling, the following conclusions can be drawn. Of the 15 theoretical interactions (different interactions occasionally yield similar curves so that the number of distinct spectra is less than 15) all but 4 may be rejected quite completely.[16] The four remaining are:

(1) Tensor Antisymmetric, with Charge Exchange

(2) Tensor, Simple Charge Exchange

(3) Scalar, Charge Retention

(4) Pseudoscalar, Charge Retention

The curves resulting from interactions (1), (3), and (4) are identical and in good agreement with the observed spectrum, as shown in Figure 9. Assuming the neutrino mass $m_\nu \cong 0$, the μ^+ meson mass corresponding to this momentum maximum is $216 \pm 8\ m_e c$. Due to the breadth of the energy resolution curve (as shown in Figure 9) the interaction (2) above still retains a certain probability. The agreement of this theoretical curve with the observed spectrum is sensitive to the actual μ meson mass. That is, calculations indicate

that while for a meson mass of $m_\mu = 216\ m_e$ interaction (2) has negligible probability, this probability increases with decreasing meson mass until for the case of $m_\mu = 206\ m_e$ its agreement with the data is 0.7 as probable as that of the other theories (1), (3), and (4). This simultaneously defines the probability of a finite upper limit for the spectrum. That these possibilities are to be considered is emphasized by a recent determination of the μ meson mass by Birnbaum, Smith, and Barkas[17] of $m_\mu = 210 \pm 2\ m_e$.

By combining several of the simple types of coupling, theoretical spectra result which range over wide latitudes. Therefore if complex combinations of more than one of the interactions are to be considered possible, the experimental curve will still leave a considerable amount of ambiguity in the identification of the combination.

For comparison, the various methods used by pervious investigators are as follows: The method of Steinberger[2] involved absorption of the positrons, i.e. a range analysis. This is a difficult approach because of the large straggling of the positrons in this momentum range. Leighton, Anderson, and Seriff,[3] employing a cloud chamber in a magnetic field, obtained 75 pictures of μ decay particles, both electrons and positrons. This small number of points when spread out over the energy spectrum result in an appreciable probable error in the final curve. Another investigation, conducted by Davis, Lock, and Muirhead[4] used the relationship between the mean square scattering angle and the energy of the particles. This method is subject to the large fluctuation of scattering, and the difficulties of the measurements in an emulsion.

The present work then has resulted in a much more accurate spectrum. Moreover, the technique of the measurement, the employment of the spectrometer and counter detection methods, is an interesting contribution to the experimental study of this problem

Acknowledgments

Dr. W. Barkas originally pointed out the possibility of this application of the spectrometer and his continuing interest helped overcome the early difficulties. Thanks are due Mr. Duane Sewell and his group for their nuclear fluxmeter measurements, and to Professor W. Powell for his extended loan of the Helmholz coils. The assistance of Mr. P. Giles on the magnet and generator adjustments is appreciated, as is the cooperation of J. Vale and the cyclotron crew.

The interest of Professor E. O. Lawrence in this research is appreciated, particularly as regards the circumstances which resulted in the availability of the spiral orbit spectrometer.

This work was performed under the auspices of the U. S. Atomic Energy Commission.

References

1. G. Miyamoto, Proc. Phys. Math. Soc. Jap. (1942)
Proc. Phys. Soc. Jap. 17, 587 (1943)
M. Sakai, J. Phys. Soc. Jap. 5, 178 (1950)

2. J. Steinberger, Phys. Rev. 75, 1136 (1949)

3. R. Leighton, C. Anderson, A. Seriff, Phys. Rev. 75, 1432 (1949)

4. J. Davis, W. Lock, H. Muirhead, Phil. Mag. 40, 1250 (1949)

5. C. Richman, and H. Wilcox, Phys. Rev. 78, 85A (1950)

6. O. Chamberlain, R. Mozley, J. Steinberger, C. Wiegand, Phys. Rev. 79, 394 (1950)

7. N. Nereson and B. Rossi, Phys. Rev. 64, 199 (1943)

8. L. Alvarez, A. Longacre, V. Ogren, R. Thomas, Phys. Rev. 77, 752A (1950)

9. S. Jones and S. White, Phys. Rev. 78, 12 (1950)

10. R. Aamodt, V. Peterson, and R. Phillips, UCRL Report No. 526

11. R. Sagane and P. Giles, Phys. Rev. 81, 653A (1950)

12. H. Friedman and J. Rainwater, Phys. Rev. 81, 644 (1951)

13. J. Tiomno, J. Wheeler and R. Rau, Rev. Mod. Phys. 21, 144 (1949)

14. L. Michel, Prod. Phys. Soc. England, 63, 514 (1950)

15. R. Serber, Phys. Rev. 75, 1459 (1949)

16. T. Green, Priv. comm.

17. W. Birnbaum, F. Smith and W. Barkas, to be published

Information Division
6/21/51 nw

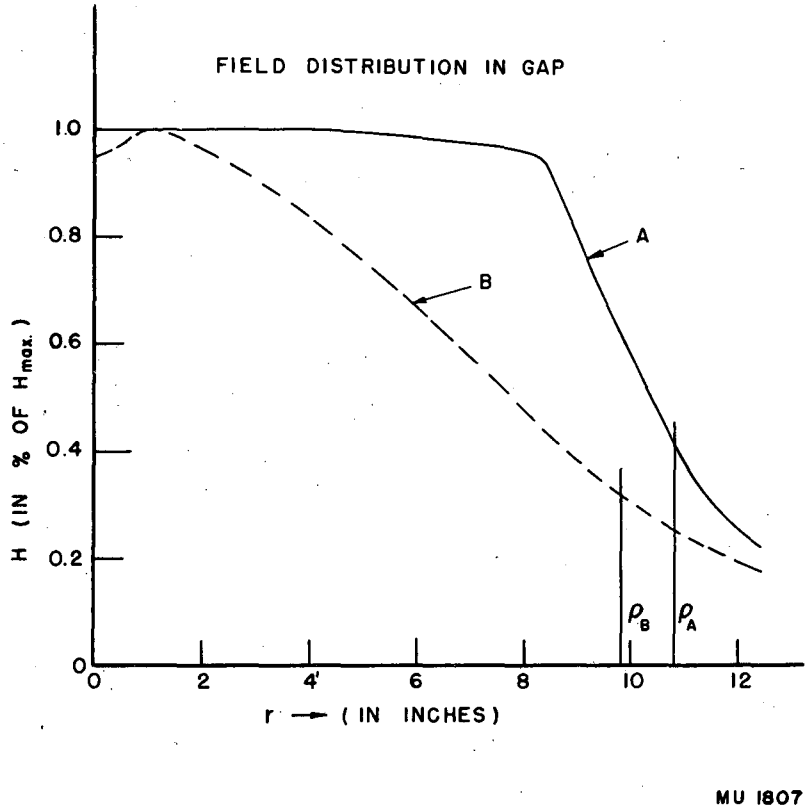
FIELD DISTRIBUTION IN GAP
1.0
0.8
0.6
0.4
0.2
0
H (IN % OF Hmax.)
A
B
ρB
ρA
0
2
4
6
8
10
12
r → (IN INCHES)
MU 1807

Fig. 1

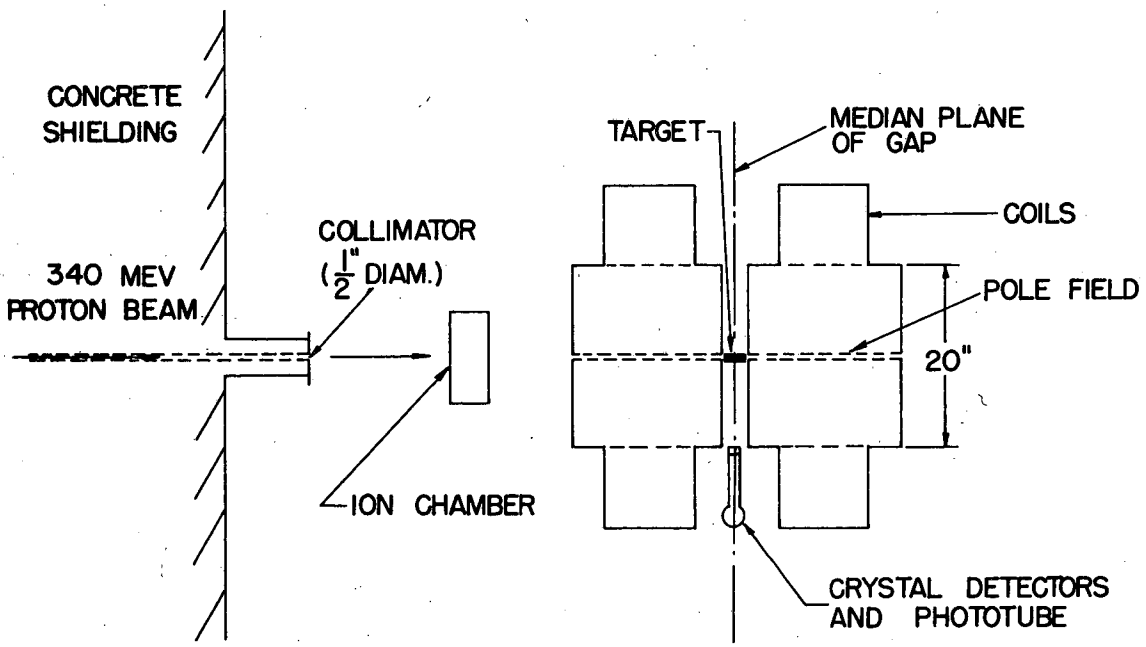
CONCRETE
SHIELDING
340 MEV
PROTON BEAM
COLLIMATOR
(1/2" DIAM.)
ION CHAMBER
TARGET
MEDIAN PLANE
OF GAP
COILS
POLE FIELD
20"
CRYSTAL DETECTORS
AND PHOTOTUBE
MU 1808

Fig. 2

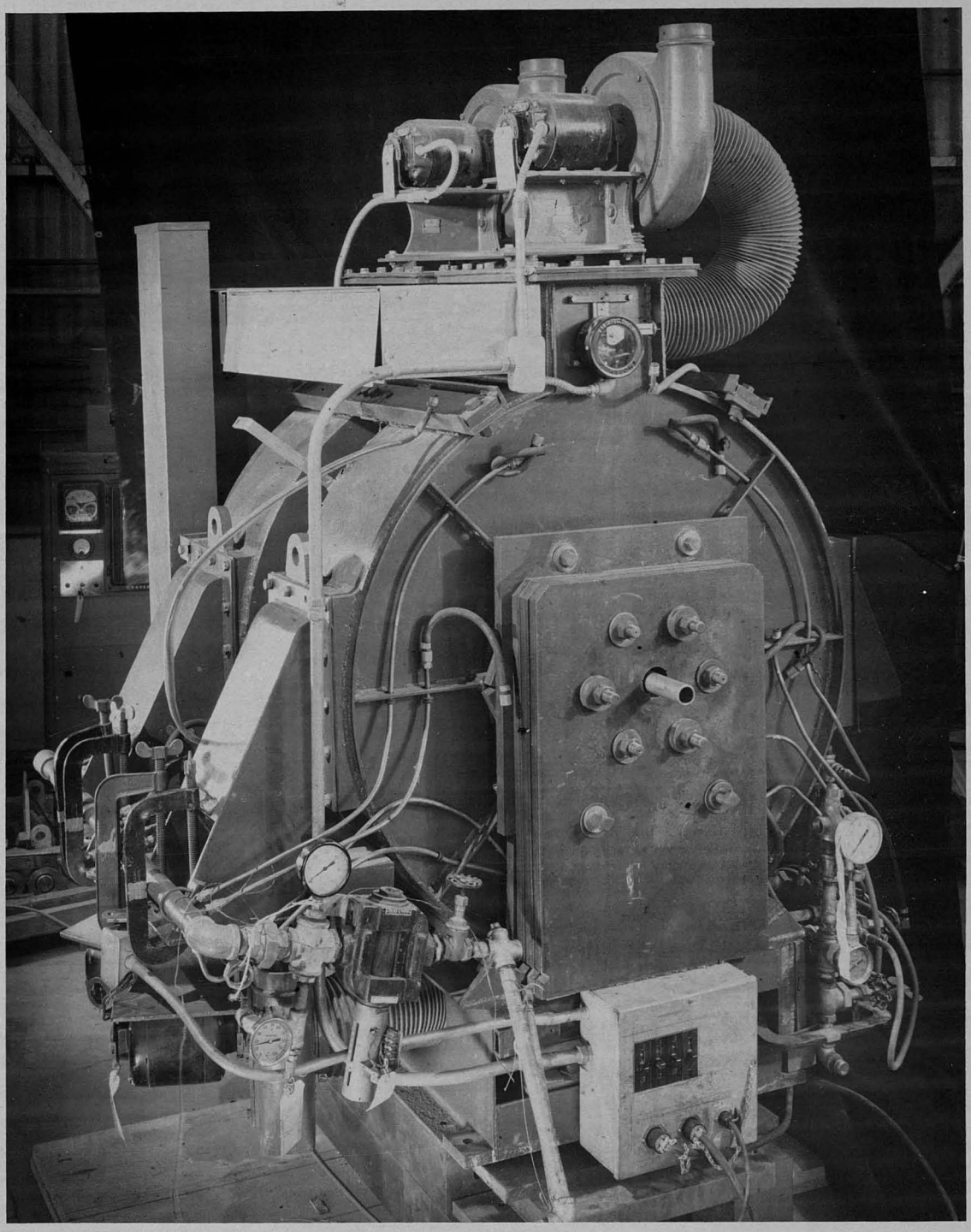

SPIRAL ORBIT SPECTROMETER

FIG. 3

SPIRAL ORBIT SPECTROMETER
MEDIAN PLANE OF GAP

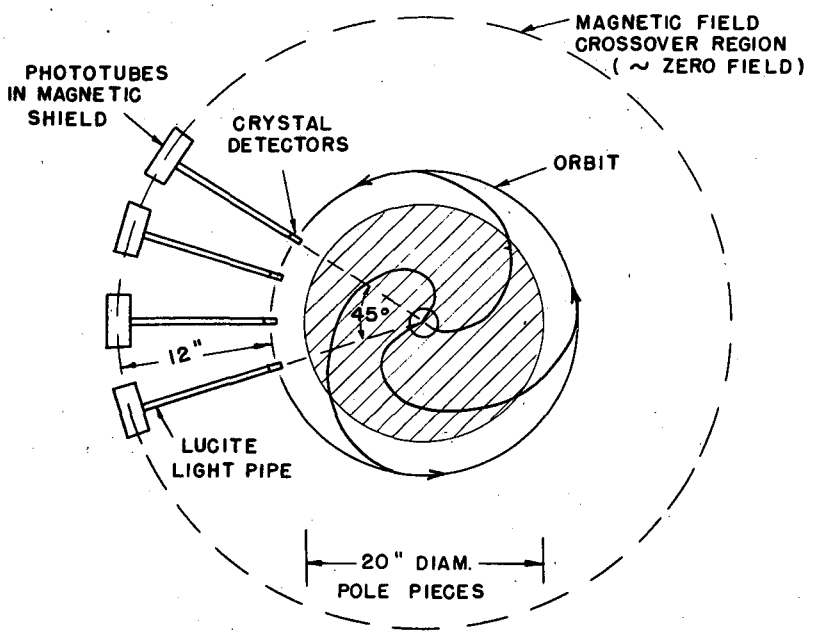

MU 1809

Fig. 4

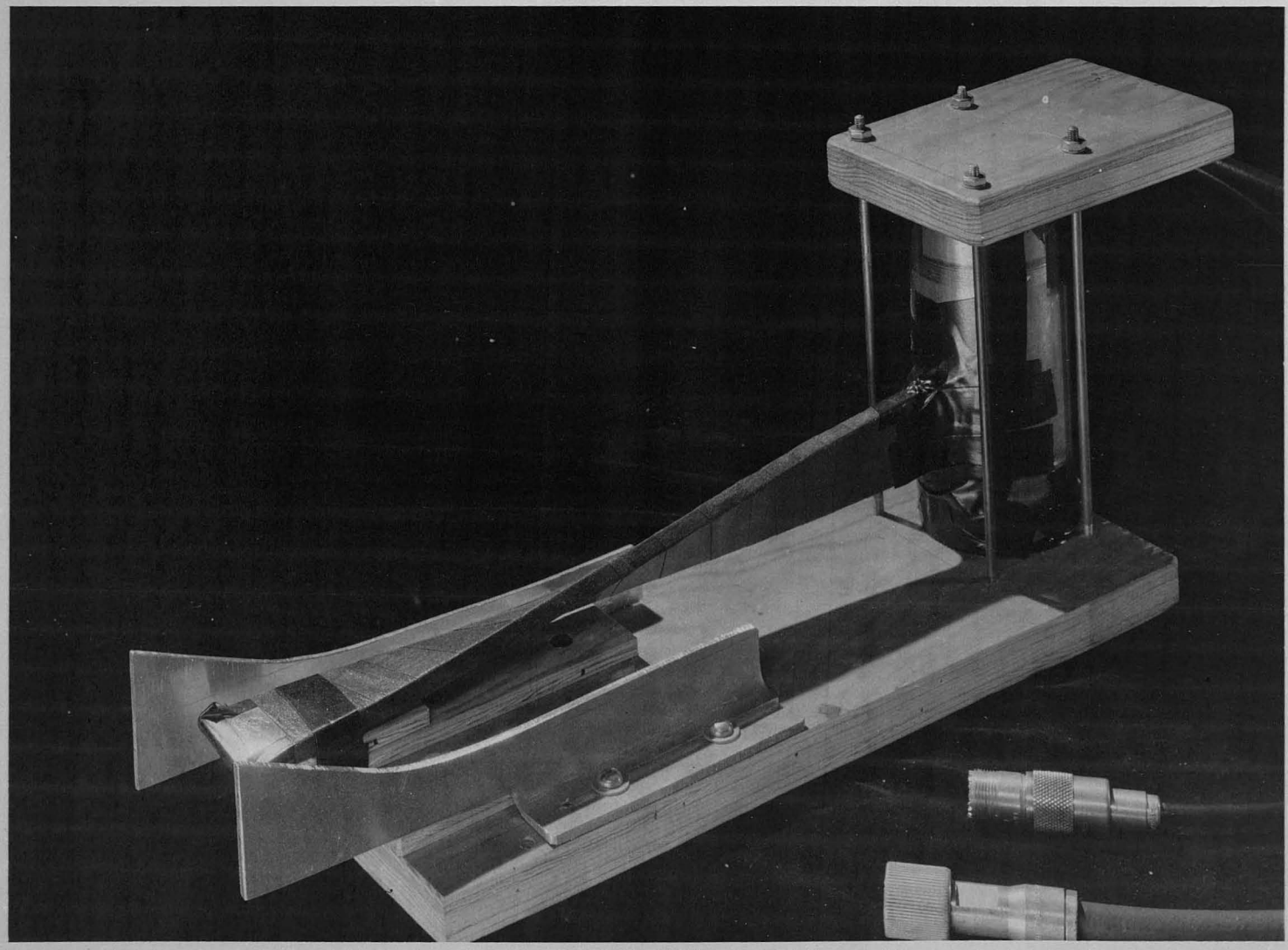

CRYSTAL AND PHOTOTUBE DETECTOR
FIG. 5

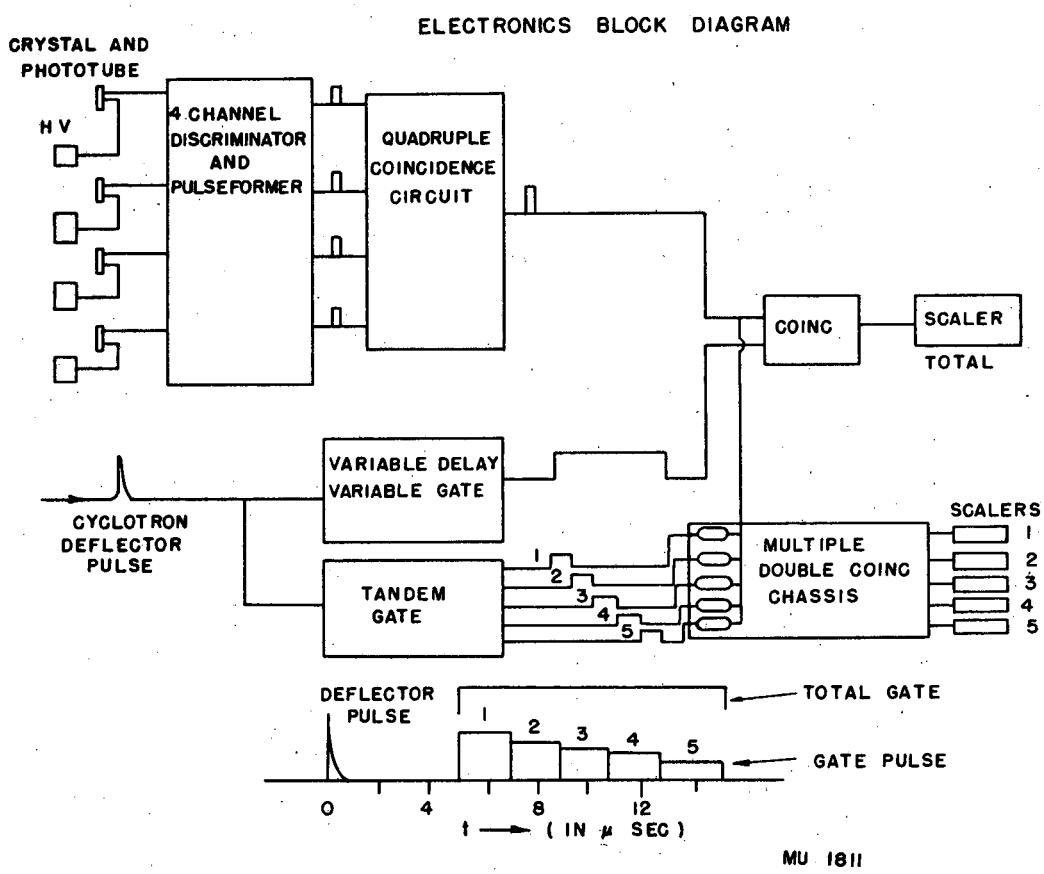
ELECTRONICS BLOCK DIAGRAM
CRYSTAL AND PHOTOTUBE
H V
4 CHANNEL DISCRIMINATOR AND PULSEFORMER
QUADRUPLE COINCIDENCE CIRCUIT
COINC
SCALER
TOTAL
VARIABLE DELAY VARIABLE GATE
CYCLOTRON DEFLECTOR PULSE
TANDEM GATE
MULTIPLE DOUBLE COINC CHASSIS
SCALERS
1
2
3
4
5
DEFLECTOR PULSE
TOTAL GATE
GATE PULSE
0
4
8
12
t → (IN μ SEC)
MU 1811

Fig. 6

BACKGROUND TESTS

A

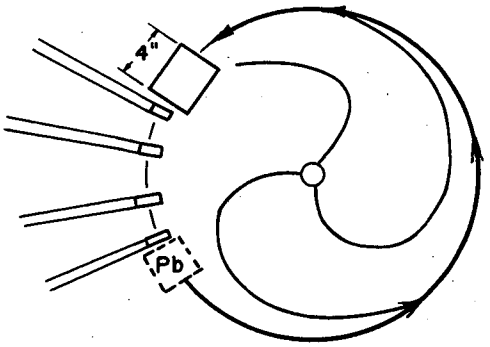

4" Pb IN PATH OF PARTICLES IN ORBIT

B

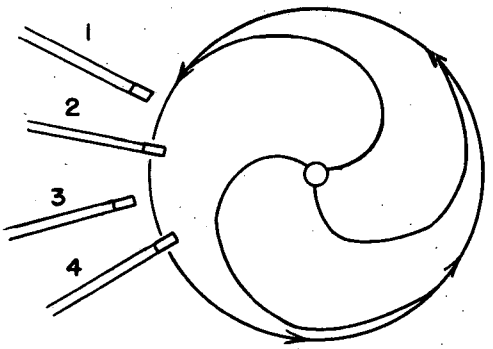

ALTERNATE CRYSTALS MOVED
1" OUT OF ORBIT

MU 1812

Fig. 7

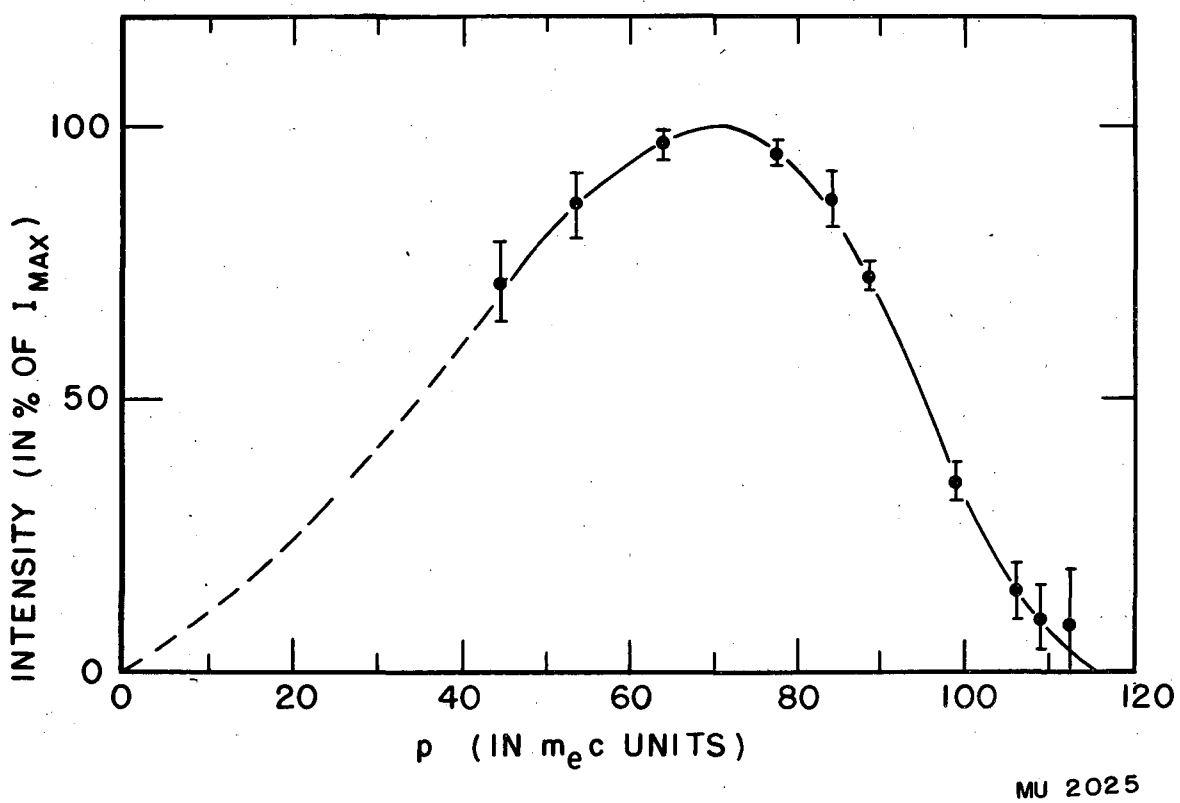
100
50
0
INTENSITY (IN % OF I_{MAX})
0
20
40
60
80
100
120
p (IN $m_e c$ UNITS)
MU 2025

Fig. 8

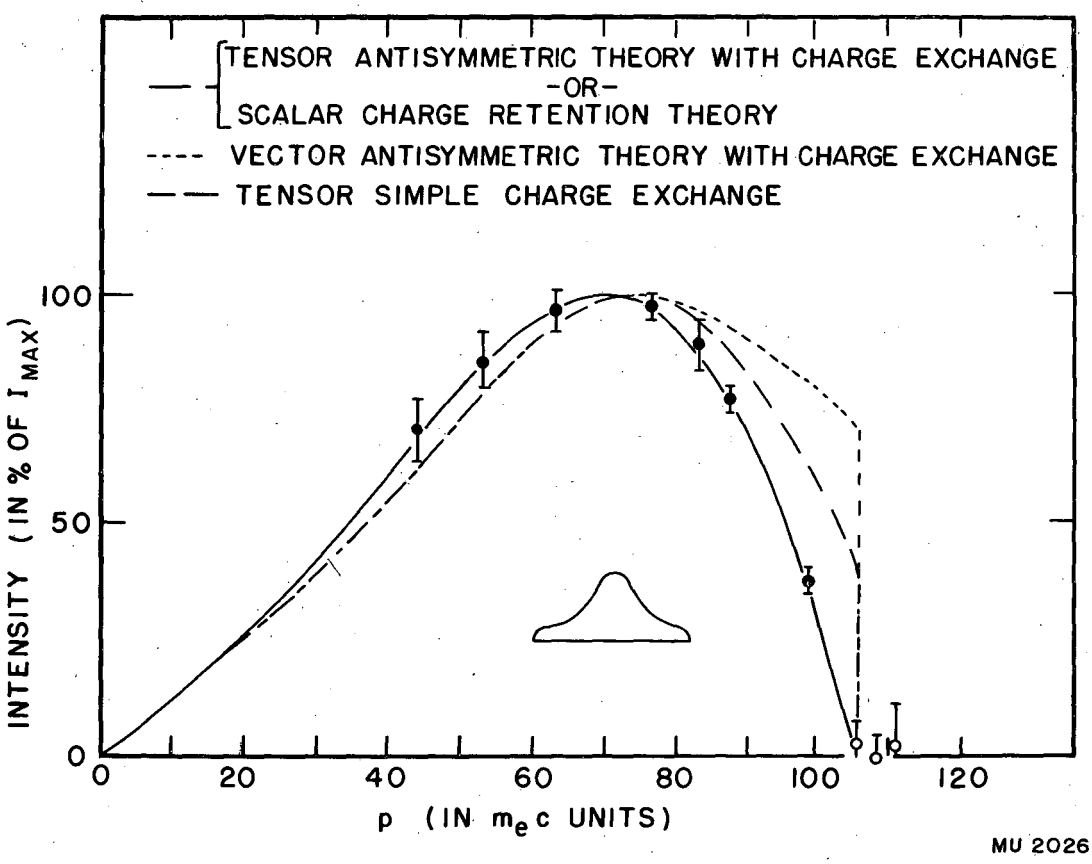
TENSOR ANTISYMMETRIC THEORY WITH CHARGE EXCHANGE
-OR-
SCALAR CHARGE RETENTION THEORY
VECTOR ANTISYMMETRIC THEORY WITH CHARGE EXCHANGE
TENSOR SIMPLE CHARGE EXCHANGE
INTENSITY (IN % OF I_{MAX})
100
50
0
0
20
40
60
80
100
120
p (IN $m_e c$ UNITS)
MU 2026

Fig. 9

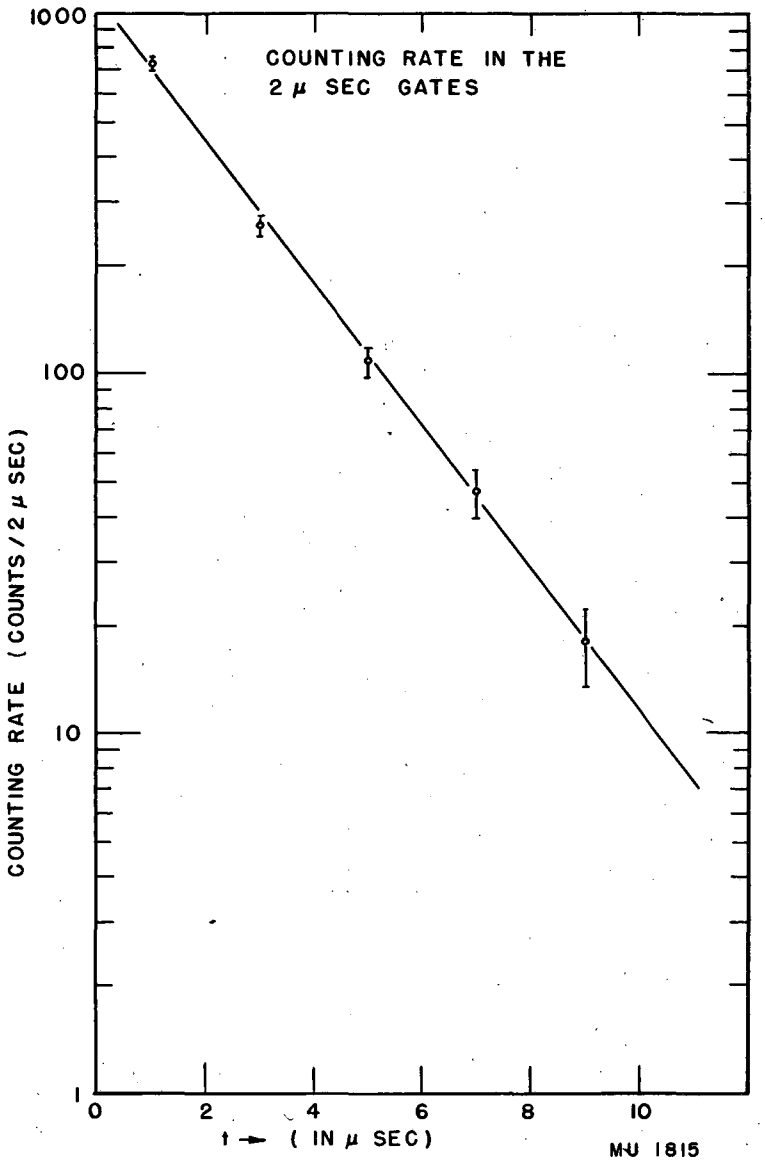
COUNTING RATE IN THE
2 μ SEC GATES
COUNTING RATE (COUNTS / 2 μ SEC)
1000
100
10
1
0
2
4
6
8
10
t → (IN μ SEC)
MU 1815

Fig. 10

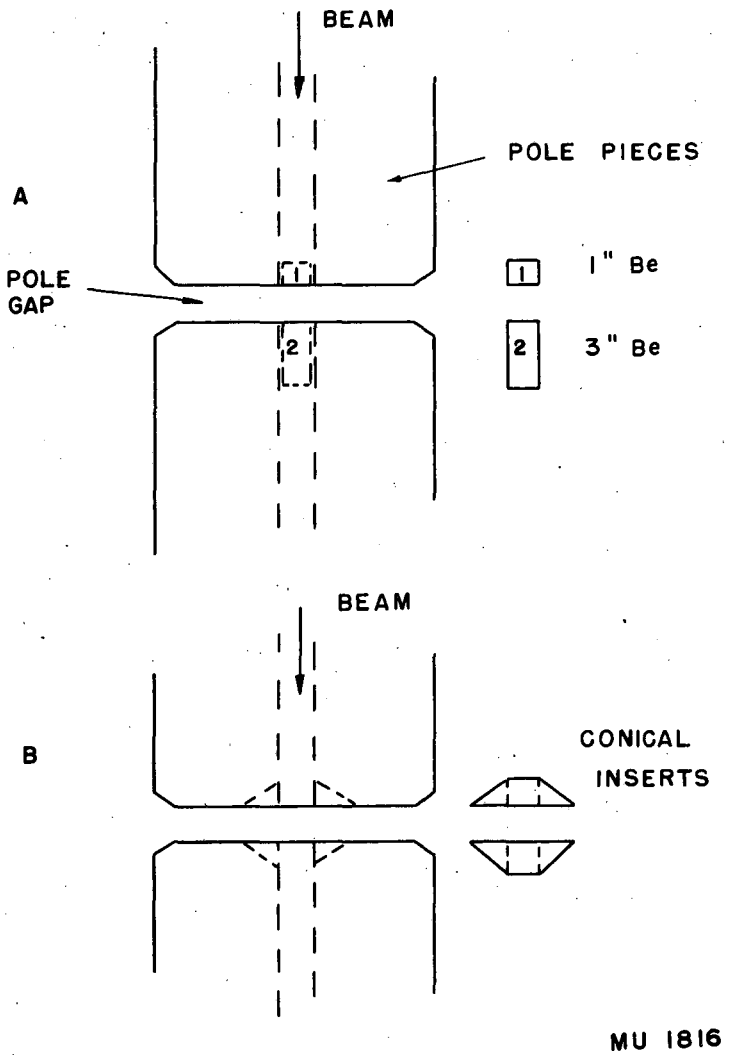
BEAM
POLE PIECES
A
POLE
GAP
1
2
1" Be
2
3" Be
BEAM
B
CONICAL
INSERTS
MU 1816

Fig. 11